

Article

HCl Removal Using Calcined Ca–Mg–Al Layered Double Hydroxide in the Presence of CO₂ at Medium–High Temperature

Wei Wu ¹, Yuanfeng Wu ² , Tongwei Wang ¹, Decheng Wang ¹, Qinyang Gu ¹ and Baosheng Jin ^{1,*}

¹ Key Laboratory of Energy Thermal Conversion and Control of Ministry of Education, School of Energy and Environment, Southeast University, Nanjing 210096, China; ww55rr44@163.com (W.W.); tongweiwang@seu.edu.cn (T.W.); dechengwang@seu.edu.cn (D.W.); guqinyang@seu.edu.cn (Q.G.)

² School of Chemistry and Chemical Engineering, Southeast University, Nanjing 210096, China; wuyuanfeng2015@163.com

* Correspondence: bsjin@seu.edu.cn; Tel.: +86-25-83794744

Received: 9 November 2019; Accepted: 20 December 2019; Published: 24 December 2019



Abstract: This present work aimed to investigate the influence of CO₂ on HCl removal using calcined Ca–Mg–Al layered double hydroxides (CaMgAl-LDHs) at medium–high temperature (400–800 °C) in a fixed-bed reactor. It was revealed that a moderate CO₂ concentration (~6%) in the flue gas of the municipal solid-waste incinerators could reduce the HCl capacity of the CaMgAl-layered double oxides (CaMgAl-LDOs). The highest capacity for HCl removal was observed over the CaMgAl-LDOs at 600 °C. However, sintering was also detected when the reaction temperature was below the calcination temperature (600 °C). Moreover, the decreasing HCl adsorption capacity of CaMgAl-LDOs was attributed to the existence of CO₂ in the flue gas, which could efficiently inhibit the decomposition of carbonates as well as the conversion into metal chloride during the HCl removal process.

Keywords: HCl; layered double hydroxide; CO₂; medium-high temperature

1. Introduction

In recent years, the output of municipal solid waste (MSW) in the world has remarkably increased alongside economic growth [1–3], especially in the developing countries. For instance, China has established many power plants fired by MSW in the past few years [4]. Although incineration is a superior energy generation waste disposal method for conserving land area, serious gas pollution and generation of solid wastes always accompany such processes. Amongst these pollutants, hydrogen chloride (HCl), a harmful gas, can do much harm not only to the human body [5–8], but also via the corrosion of the incinerator and pipes [9,10]. It has been reported that at medium–high temperature (250–450 °C), HCl can be efficiently converted into polychlorinated dibenzodioxins (PCDDs) and polychlorinated dibenzofurans (PCDFs) [11,12]. Unfortunately, PCDDs and PCDFs are detrimental to the environment and to human health in general. Therefore, it is necessary to remove HCl at medium–high temperature, preferably above 500 °C, to prevent these highly toxic chlorinated compounds from being formed. Wet, dry, and semi-dry methods for the removal of HCl have been widely studied, with the dry method being superior to the other two, considering the operating temperature range and difficulties in sludge handling [13–15]. In addition, different types of sorbents, such as CaO-based [7,16–18], MgO-based [19,20], and sodium sorbents [21–23], have been used to remove HCl; however, most cases showed generally poor performance for HCl removal, especially at high temperatures.

Layered double hydroxides (LDHs) have attracted increasing attention based on their large interlayer surface area and potential applications, including as adsorbents, catalysts, and catalyst

supports [24–29]. The general structural formula of hydrotalcite-like samples (HTLs) can be written as $[M^{2+}_{1-x}M^{3+}_x(OH)_2]^{x+}[A^{n-}_{x/n}]^{x-}\cdot zH_2O$, where M^{2+} (such as Mg^{2+} , Ca^{2+} , Zn^{2+}) and M^{3+} (Al^{3+} , Fe^{3+} , etc.) are divalent and trivalent cations, respectively. The value of x is equal to the molar ratio of $M^{3+}/(M^{2+} + M^{3+})$, and A is an interlayer anion of valence, n [30]. The layered double oxides (LDOs), which possess higher specific surface areas and more active sites, can be obtained by calcining the LDHs [31]. In our previous reports, some LDOs, such as Ca–Mg–Al, Ca–Zn, and Mg–Fe LDOs [5,32,33], were found to have high HCl adsorption capacity, and efficient removal capacity due to the newly-formed metal oxides during the pretreatment [6,7].

CO_2 is the main content of the flue gas produced during MSW combustion, and can react with CaMgAl-LDOs. Therefore, it is expedient to study the influence of CO_2 on the HCl adsorption capacity of CaMgAl-LDOs. In this work, the CaMgAl-LDHs were fabricated via co-precipitation method, while the calcined samples were applied to remove HCl in flue gas in the presence of CO_2 . The effects of calcination temperature, reaction temperature, CO_2 concentration, initial HCl concentration, particle size, and gas flow rate on the efficiency of HCl removal were studied. Moreover, characterizations including X-ray powder diffraction (XRD), scanning electron microscopy (SEM), and thermal gravimetric (TG) analyzer were employed to reveal the relationship between the adsorption capacity and characteristic properties of the CaMgAl-LDOs.

2. Results and Discussion

2.1. Characterization of the As-Synthesized Samples

Figure 1 depicts the XRD patterns of as-prepared CaMgAl-LDHs calcined at different temperatures between 550 °C and 800 °C, with that of CaMgAl-LDH as reference. It can be seen that the CaMgAl-LDH contains two different layered double hydroxides, i.e., $Mg_{0.677}Al_{0.333}(OH)_2(CO_3)_{0.167}\cdot 0.5H_2O$ and $Ca_{0.68}Al_{0.32}(OH)_2(CO_3)_{0.16}\cdot 0.47H_2O$, which were converted into $CaCO_3$ and $Mg_{0.03}Ca_{0.97}(CO_3)$ after being calcined at ~550–650 °C. However, no Al-containing compound was detected, which may have existed in the amorphous state. When the samples were calcined above 750 °C, Ca-based and Mg-based carbonates ($CaCO_3$, $Mg_{0.03}Ca_{0.97}(CO_3)$) disappeared, forming the corresponding oxide states (CaO , MgO , and $Ca_5Al_6O_{14}$). It is worth mentioning that calcium carbonates, including calcite and aragonite, were formed within the synthesized samples, both of which can provide the CaMgAl-LDOs with good thermal stability, solubility, and specific surface area.

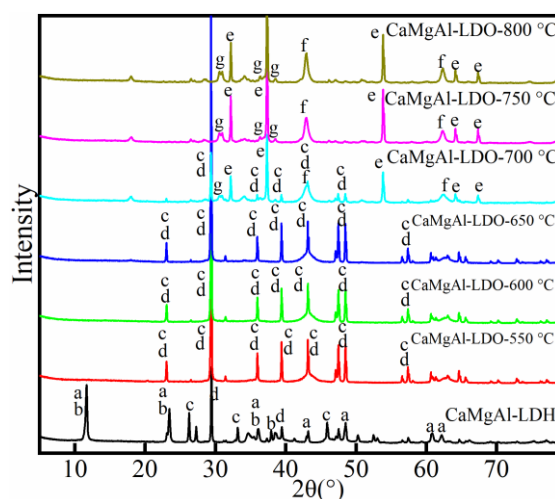


Figure 1. XRD patterns of as-prepared CaMgAl-LDHs calcined at different temperatures from 550 °C to 800 °C. (a) $Mg_{0.677}Al_{0.333}(OH)_2(CO_3)_{0.167}\cdot 0.5H_2O$; (b) $Ca_{0.68}Al_{0.32}(OH)_2(CO_3)_{0.16}\cdot 0.47H_2O$; (c) $CaCO_3$; (d) $Mg_{0.03}Ca_{0.97}(CO_3)$; (e) CaO ; (f) MgO ; (g) $Ca_5Al_6O_{14}$.

In order to elucidate the microstructure of the Ca–Mg–Al layered double hydroxides calcined at different temperatures, the morphologies of the samples were characterized by SEM, as shown in Figure 2. For the fresh sample shown in Figure 2a, the particles of the CaMgAl-LDHs were covered with uniformly sized of grains at about 1 μm , while also revealing some porous structures on the surface. After calcination at 550 $^{\circ}\text{C}$ (Figure 2b), the grains of LDOs on the particle surface was converted into rod-like shapes due to the decomposition of the CaMgAl-LDHs, resulting in a more porous structure and higher specific surface area. As can be seen in Figure 1, the CaMgAl-LDHs decomposed into CaCO_3 and $\text{Mg}_{0.03}\text{Ca}_{0.97}(\text{CO}_3)$ when the calcination temperature reached 550 $^{\circ}\text{C}$. As the calcination temperature increased to 600 $^{\circ}\text{C}$ (Figure 2c), the pores became even more developed and prominent, although a large quantity of grains aggregated together due to sintering. Further increase of the temperature resulted in the sintering of LDOs becoming more serious and the porous structure on the surface of the particle gradually disappearing (Supplementary Table S1). Based on the porous structure mentioned earlier, the LDHs calcined at 600 $^{\circ}\text{C}$ were chosen for further research.

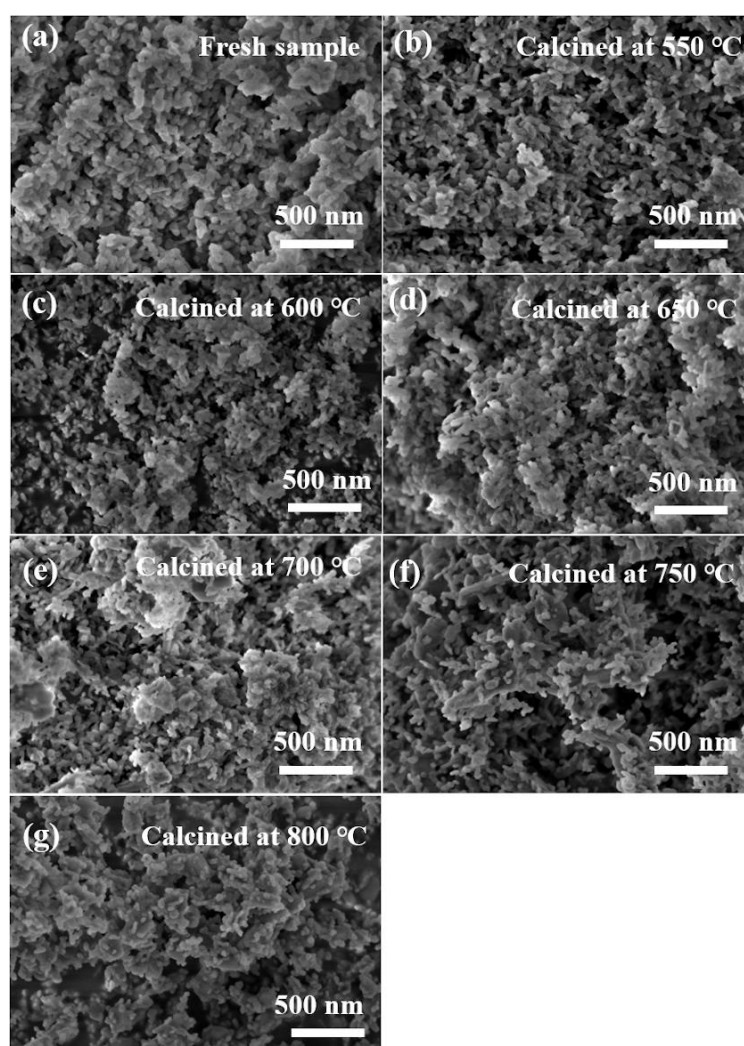


Figure 2. SEM images of Ca–Mg–Al layered double hydroxides calcined at different temperatures: (a) fresh sample; (b) calcined at 550 $^{\circ}\text{C}$; (c) calcined at 600 $^{\circ}\text{C}$; (d) calcined at 650 $^{\circ}\text{C}$; (e) calcined at 700 $^{\circ}\text{C}$; (f) calcined at 750 $^{\circ}\text{C}$; (g) calcined at 800 $^{\circ}\text{C}$.

The thermal stability was a critical factor to evaluate for the synthesized samples. The TG/DTG profiles of CaMgAl-LDHs were recorded from 30 to 800 $^{\circ}\text{C}$ (10 $^{\circ}\text{C min}^{-1}$), with nitrogen being employed as the protective gas (Figure 3). The TG profile was generally divided into three stages in reference to

the DTG curve. About 10% weight loss was detected for Stage I between 100 °C and 250 °C, which was ascribed to the removal of physically adsorbed and interlayer water [34]. Stage II, appearing in the temperature range between 250 °C and 460 °C, was associated with the dehydroxylation of brucite-like sheets as well as the partial decomposition of carbonate groups [35]. Moreover, at Stage III, a large weight loss occurred in the range of 600 °C to 770 °C, which was due to decomposition of the carbonates at high temperatures.

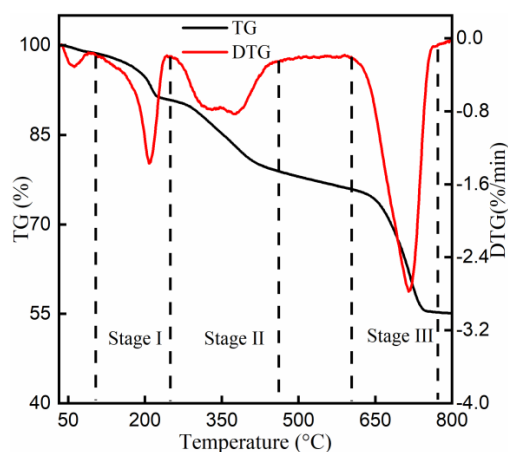


Figure 3. TG/DTG profiles of CaMgAl-LDHs.

In order to study the efficiency of CO₂ on the removal performance, the TG profiles of CaMgAl-LDOs treated at 600 °C were recorded in 6% CO₂/N₂ and N₂ atmospheres (Figure 4). It was clearly seen that TG profiles were almost equal before 600 °C. However, the two TG curves exhibited an obvious difference above 600 °C, with the TG curve of the CaMgAl-LDOs in N₂ atmosphere exhibiting a downtrend after 600 °C, a phenomenon which was attributed to the decomposition of the carbonate anions. Furthermore, as can be seen in Figure 1, CaO and MgO were both formed after 650 °C, which was ascribed to the decomposition of CaCO₃ and Mg_{0.03}Ca_{0.97}(CO₃). Additionally, the TG profile of CaMgAl-LDOs in the CO₂/N₂ atmosphere was almost kept constant, since the CO₂/N₂ atmosphere enhanced the partial pressure of CO₂, hindering the decomposition of the carbonate anions.

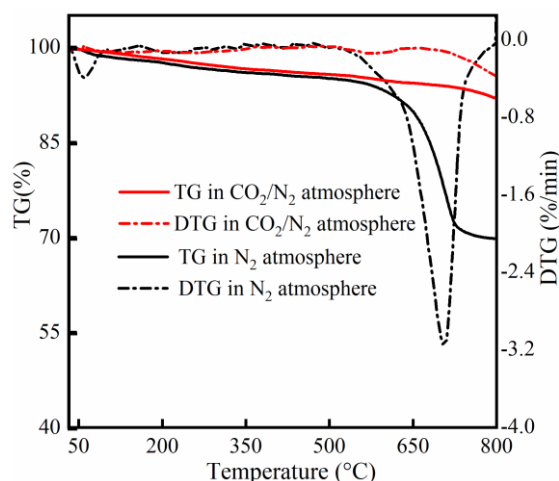


Figure 4. TG profiles of CaMgAl-LDOs in a 6% CO₂/N₂ and N₂ atmosphere.

2.2. Effect of CO₂ Concentration on HCl Removal

Figure 5 shows the HCl removal capacity at different CO₂ concentrations, measured in order to study the influence of CO₂ concentration on the adsorption of HCl for the CaMgAl-LDOs. As the CO₂ concentration increased from 0% to 16%, the HCl capacity decreased from 0.201 g to 0.161 g, with the

breakthrough time (when C_{out} is equal to C_{in}) reducing from 497 min to 390 min. In other words, the HCl capacity decreased by 21.53%, and the breakthrough time reduced by 18.75%. Moreover, when the CO_2 concentration increased from 0% to 2%, the HCl capacity and breakthrough time decreased by 8.98% and 9.26%, respectively. However, both the HCl capacity and breakthrough time remained almost constant as the CO_2 concentration increased from 2% to 10%. Thereafter, the HCl capacity and breakthrough time continued to drop by 13.52% and 9.83% as the CO_2 concentration further increased to 12%, after which the HCl capacity and breakthrough time remained almost unchanged with the CO_2 concentration increase from 12% to 16%.

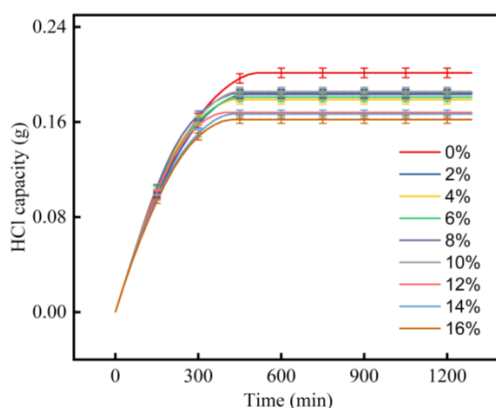


Figure 5. HCl removal capacity using different CO_2 concentrations.

From the above analysis and discussion, it was concluded that the CO_2 concentration has a moderate influence on the HCl capacity and breakthrough time of the CaMgAl-LDOs. Considering the presence of CO_2 and its concentration level (~6%) in the flue gas of the municipal solid-waste incinerators, it is meaningful to investigate the influence of CO_2 concentration on HCl removal. As a result, the CO_2 concentration of 6% was selected for further analysis.

2.3. Effect of HCl Concentration on Its Removal

Figure 6 depicts the HCl removal capacity of LDOs at different HCl concentrations. It can be seen that the HCl breakthrough timing of CaMgAl-LDO showed a downtrend with increasing HCl concentrations. For example, the HCl breakthrough time reduced from about 1000 min to 500 min as the HCl concentration increased from 250 ppm to 500 ppm. When the HCl concentration was more than 750 ppm, the HCl removal adsorption curves were almost constant. It is obvious that the reaction rate was controlled by the chemical dynamics, while the HCl removal rate was determined by the diffusion rate of HCl to the surface of the CaMgAl-LDO particles. Ultimately, the HCl removal capacity of LDOs was equal at different HCl concentrations.

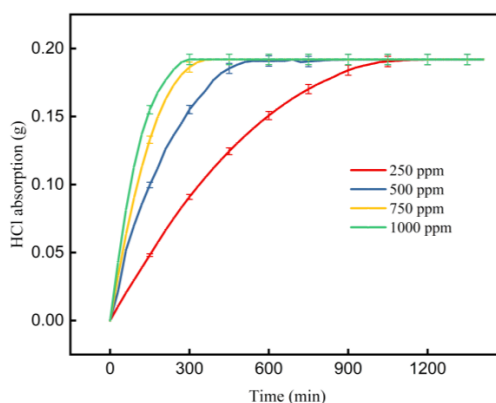


Figure 6. HCl removal capacity with different HCl concentrations under CO_2 concentration of 6%.

2.4. Effect of Particle Size of the LDOs on HCl Removal

Figure 7 shows the HCl removal capacity with different particle sizes of the LDOs. With the decrease in particle size, both the HCl removal capacity and removal rate increased, which could have been due to the increasing exposure of active sites able to efficiently adsorb the HCl molecules, because the product layer of $\text{CaCl}_2 \cdot 2\text{H}_2\text{O}$ would hinder the adsorption of HCl molecules through the pores of the particle. Moreover, in order to slow the arrival of the HCl breakthrough time, the particle size of 150–212 μm was selected for further investigations.

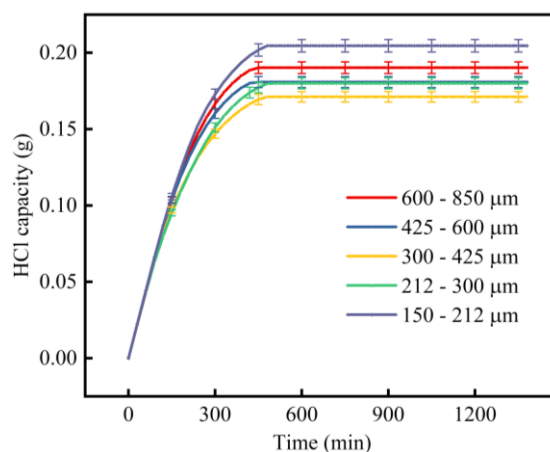


Figure 7. HCl removal capacity with different particle sizes of CaMgAl-LDOs.

2.5. Effect of Gas Velocity on HCl Removal

Figure 8 demonstrates the HCl removal capacity at different gas velocities from 0.7 to 1.3 L/min. As the gas velocity increased from 0.7 to 1.3, the HCl removal capacity and breakthrough time simultaneously increased. However, when the gas velocity reached 1.3 L/min, the HCl removal capacity obviously decreased, which could have been attributed to the increasing outflow of the CaMgAl-LDOs under high gas velocity (above 0.9 L/min). In other words, the decrease in the amount of the sample was the direct reason for the decrease of HCl capacity. Hence, a gas velocity of 0.9 L/min was applied for the subsequent experiments.

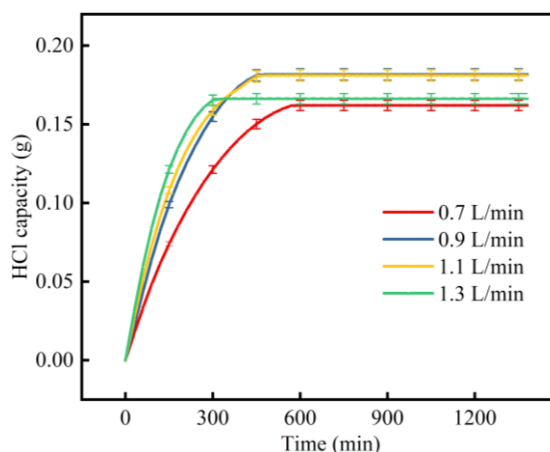


Figure 8. HCl removal capacity at different gas velocities.

2.6. Effect of Reaction Temperature on HCl Removal

The HCl removal capacity at different reaction temperatures is depicted in Figure 9. It can be seen that the HCl removal capacity increased as the temperature increased from 400 $^{\circ}\text{C}$ to 600 $^{\circ}\text{C}$,

followed by a decrease with further temperature increase from 600 °C to 800 °C. CaO possesses an abundant porous structure, making it a better HCl sorbent than CaCO₃, while Ca, Mg, and Al oxides can be transformed into unreactive oxides (Ca₅Al₆O₁₄). In addition, sintering often occurred at high temperatures, which could have resulted in a decreasing removal capacity for HCl adsorption. Therefore, high temperature is not recommended for the HCl removal using CaMgAl-LDOs, as the highest removal performance was observed at 600 °C, where the HCl removal capacity reached 0.181 g.

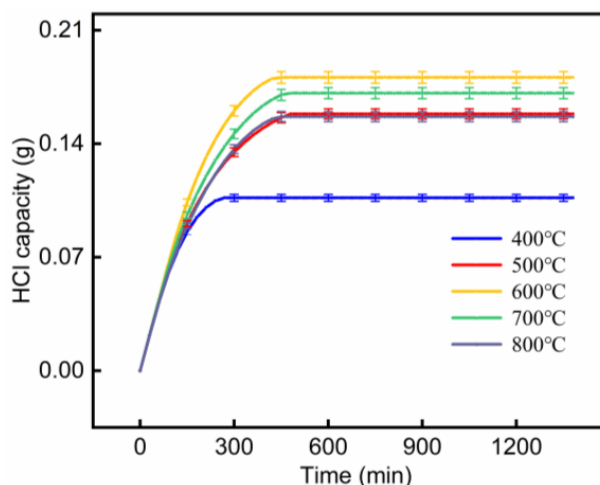


Figure 9. HCl removal capacity at different reaction temperatures.

2.7. Morphology and Components

Figure 10 depicts the SEM images of different CaMgAl-LDOs collected at different working temperatures. Grains with a size of 1 µm over the particle surface resulted into a porous structure for the fresh sample as seen in Figure 10a, while the microstructure of the CaMgAl-LDOs changed largely for all the recovered samples undergoing different reaction temperatures. In the range of 400–600 °C, the grains of CaMgAl-LDOs increasingly agglomerated together, leading to a decrease in specific surface area (Supplementary Table S1). This phenomenon indicated that when the temperature was lower than the calcination temperature of 600 °C, sintering could also occur. At temperatures higher than 600 °C, the microstructure of the CaMgAl-LDOs collapsed terribly, resulting in the growth and tight agglomeration of the grains, which consequently blocked the pores and inhibited adequate contact between HCl and the samples. Therefore, the change of morphology observed for the recovered samples can be attributed both to sintering effect and to phase transformation (Figure 11). Additional supports (e.g., porous inert alumina, magnesium aluminate) with anti-sintering properties are recommended to employ to further improve the reactivity and adsorption capacity of the CaMgAl-LDOs.

Figure 11 illustrates the XRD patterns of the recovered CaMgAl-LDOs at different reaction temperatures between 400 °C and 800 °C. It can be observed that CaCl₂·2H₂O and MgCl₂ were the main products of CaMgAl-LDOs and HCl. With the increase in the reaction temperature, the intensity of the diffraction peak of CaCO₃ remarkably decreased, which was associated with the decomposition of carbonate within CaMgAl-LDOs. Additionally, it was found that the CaCO₃ remained incompletely decomposed at 800 °C, which may have been due to the CO₂ in the inlet gas. More importantly, the method for regenerating the sorbent (CaMgAl-LDOs) is also interesting for future sustainable development.

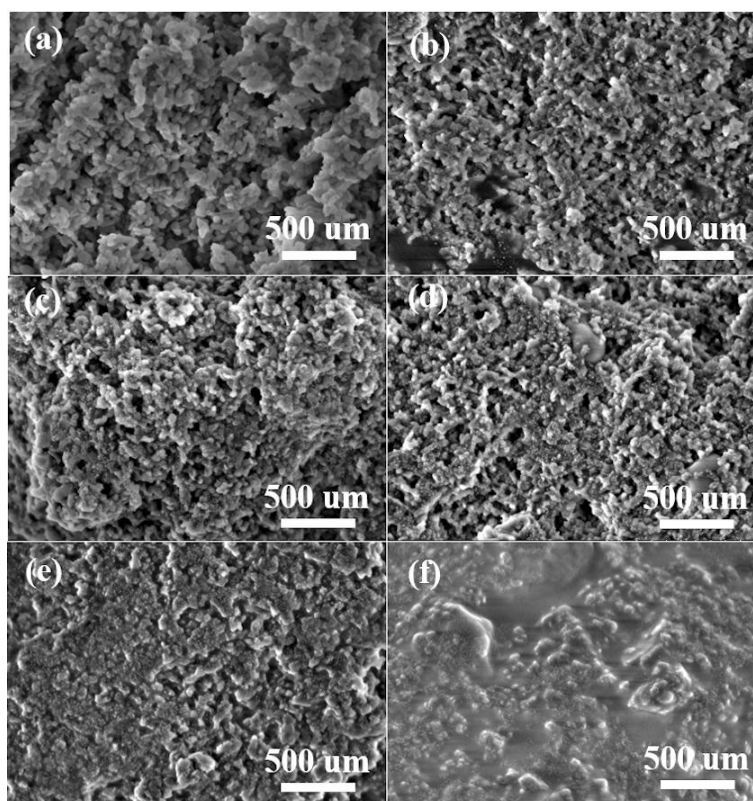


Figure 10. SEM images of recovered CaMgAl-LDOs at different reaction temperatures: (a) fresh sample; (b) at 400 °C; (c) at 500 °C; (d) at 600 °C; (e) at 700 °C; (f) at 800 °C.

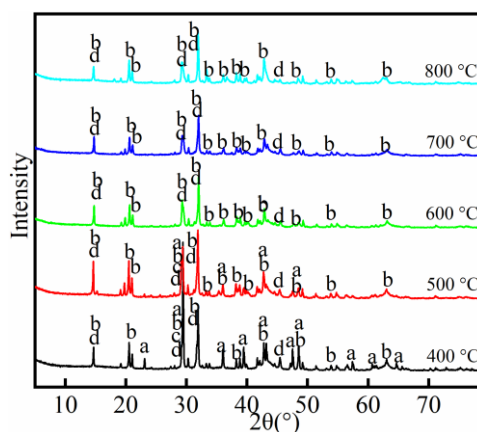


Figure 11. XRD patterns of recovered CaMgAl-LDOs at different reaction temperatures between 400 °C and 800 °C. (a) CaCO_3 ; (b) $\text{CaCl}_2 \cdot 2\text{H}_2\text{O}$; (c) $\text{Mg}_{0.03}\text{Ca}_{0.97}(\text{CO}_3)$; (d) MgCl_2 .

3. Materials and Methods

3.1. Synthesis of Ca–Mg–Al LDOs

The co-precipitation method was adopted for the synthesis of the Ca–Mg–Al LDHs. The precipitant solution, including Na_2CO_3 (1.5 mol), NaOH (2.0 mol), and the metal salt solutions ($\text{Ca}(\text{NO}_3)_2 \cdot 4\text{H}_2\text{O}$ (0.4 mol), $\text{Mg}(\text{NO}_3)_2 \cdot 6\text{H}_2\text{O}$ (0.4 mol), and $\text{Al}(\text{NO}_3)_3 \cdot 9\text{H}_2\text{O}$ (0.2 mol)), were simultaneously added into 300 mL deionized (DI) water, after which the system was heated at 60 °C. During the preparation process, the pH was kept almost constant (10.5). After the system was heated for 24 h, another 12 h was allowed for aging. Subsequently, the precipitate was filtered and washed with DI water several times until the pH reached 7, and the obtained precipitate was labeled as CaMgAl-LDHs.

After further calcination at 600 °C, the metal oxides (named CaMgAl-LDOs) were ground and sieved to different particle sizes (150–212, 212–300, 300–425, 425–600, and 600–850 µm) for the dechlorination test. To investigate the effects of calcination temperature on the adsorption performance as well as physiochemical properties, the CaMgAl-LDHs were treated at different temperatures (550, 600, 650, 700, 750, and 800 °C) for comparative studies.

3.2. Characterizations

X-ray powder diffraction (XRD) was performed with a Rigaku Ultima IV with a Cu-K α radiation at a rate of 10°/min, while the scanning electron microscopy (SEM) was carried out on a Hatchi Regulus 8220 (EDX, Oxford Instruments Ultim Extreme). Moreover, the thermal gravimetric behaviors were measured using a NETZSCH STA 449F3 instrument, after which the instrument was also used to study the influence of CO₂ on the reactivity and mass change of the CaMgAl-LDOs.

3.3. Experimental Reactor and Procedure

The adsorption test was carried out in a vertical fixed quartz tubular reactor (Figure 12). In each test, 0.5 g sample was evenly discharged into the quartz glass tube, after which the sample was further heated to the target temperature (400, 500, 600, 700, or 800 °C) with 0.75 L/min nitrogen as protective gas. The HCl gas (3000 ppm) was then sent into the reactor (0.15 L/min), and was adsorbed by the heated sample. The residual HCl concentration was then analyzed by a Model 7900FM HCl GFC analyzer online, followed by being thoroughly adsorbed using NaOH solution.

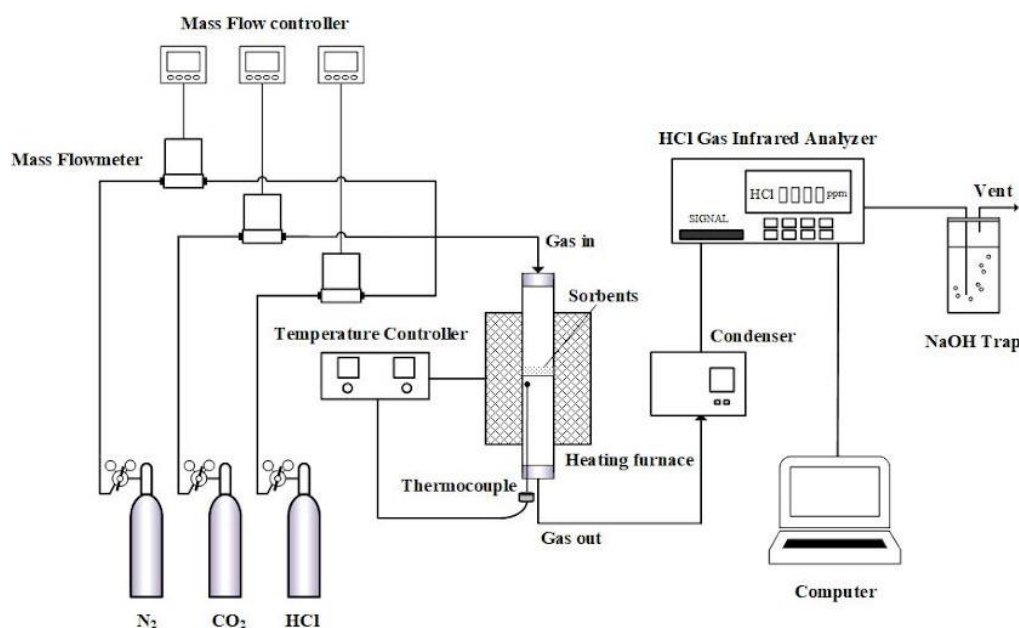


Figure 12. Schematic diagram of the experimental setup.

3.4. Data Evaluation

The removal efficiencies and adsorption capacity were adopted as the important criteria for evaluating the adsorption performance of the CaMgAl-LDOs, which were calculated according to the following Equations (1) and (2), respectively.

$$\eta = \left(\frac{C_{in} - C_{out}}{C_{in}} \right) \times 100\%, \quad (1)$$

$$q_T = \int_0^T (C_{in} - C_{out}) \times \frac{M}{22.4} \times 10^{-6} V dt \quad (2)$$

where η (removal efficiency) and q_T (cumulative adsorption mass of HCl) can be calculated according to the following parameters: C_{in} (concentration of HCl in inlet gas), C_{out} (concentration of HCl in outlet gas), T (reaction time), V (the flow velocity of the mixed gases), and M (relative molecular mass).

4. Conclusions

The influence of CO₂ on HCl removal using CaMgAl-LDOs was analyzed at medium–high temperatures (400–800 °C) in a fixed-bed reactor. It was discovered that the LDHs calcined at 600 °C possessed the most developed porous structure, while the CaMgAl-LDOs with smaller particles possessed higher HCl removal capacity in the presence of CO₂. The moderate CO₂ concentration (~6%) in the flue gas of the municipal solid-waste incinerators could lessen the HCl capacity of the CaMgAl-LDOs. When the reaction temperature was maintained at 600 °C, the highest adsorption capacity of the CaMgAl-LDOs was observed. Moreover, sintering occurred easily when the reaction temperature was lower than the calcination temperature (600 °C), while the CO₂ in the flue gas could also prevent the decomposition of carbonates.

Supplementary Materials: The following are available online at <http://www.mdpi.com/2073-4344/10/1/22/s1>, Table S1: BET Surface Area and Pore-size Distribution for CaMgAl-LDOs at different conditions.

Author Contributions: Conceptualization, W.W. and B.J.; methodology, W.W. and Y.W.; validation, B.J.; formal analysis, W.W. and Q.G.; investigation, W.W., T.W., D.W. and Q.G.; resources, W.W., T.W. and D.W.; data curation, W.W. and Y.W.; writing, original draft preparation, W.W.; writing, review and editing, W.W. and B.J.; funding acquisition, B.J. All authors have read and agreed to the published version of the manuscript.

Funding: The research was funded by the National Key R&D Program of China [2018YFC1901200], The National Natural Science Foundation of China [51741603].

Conflicts of Interest: The authors declare no conflict of interest. The funders have no role in the design of the study, collection, analysis or interpretation of data and also in the writing of the manuscript as well as the decision to publish the results.

References

1. Li, H.; Gao, P.; Ni, H. Emission characteristics of parent and halogenated PAHs in simulated municipal solid waste incineration. *Sci. Total Environ.* **2019**, *665*, 11–17. [[CrossRef](#)] [[PubMed](#)]
2. Zhou, Q.; Yang, J.; Liu, M.; Liu, Y.; Sarnat, S.; Bi, J. Toxicological risk by inhalation exposure of air pollution emitted from China's municipal solid waste incineration. *Environ. Sci. Technol.* **2018**, *52*, 11490–11499. [[CrossRef](#)] [[PubMed](#)]
3. Beylot, A.; Hochar, A.; Michel, P.; Descat, M.; Ménard, Y.; Villeneuve, J. Municipal solid waste incineration in France: An overview of air pollution control techniques, emissions, and energy efficiency. *J. Ind. Ecol.* **2018**, *22*, 1016–1026. [[CrossRef](#)]
4. Ji, L.; Lu, S.; Yang, J.; Du, C.; Chen, Z.; Buekens, A.; Yan, J. Municipal solid waste incineration in China and the issue of acidification: A review. *Waste Manag. Res.* **2016**, *34*, 280–297. [[CrossRef](#)] [[PubMed](#)]
5. Cao, J.; Chen, T.; Jin, B.; Huang, Y.; Hu, C. Adsorption of HCl on calcined Ca and Zn hydrotalcite-like compounds (HTLs) at medium-high temperature in flue gas. *Ind. Eng. Chem. Res.* **2019**, *58*, 18–26. [[CrossRef](#)]
6. Li, Y.; Wang, W.; Cheng, X.; Su, M.; Ma, X.; Xie, X. Simultaneous CO₂/HCl removal using carbide slag in repetitive adsorption/desorption cycles. *Fuel* **2015**, *142*, 21–27. [[CrossRef](#)]
7. Chyang, C.; Han, Y.; Zhong, Z. Study of HCl absorption by CaO at high temperature. *Energy Fuel* **2009**, *23*, 3948–3953. [[CrossRef](#)]
8. Shi, J.; Hui, F.; Yuan, J.; Yu, Q.; Mei, S.; Zhang, Q.; Li, J.; Wang, W.; Yang, J.; Lu, J. Ru-Ti oxide based catalysts for HCl oxidation: The favorable oxygen species and influence of Ce additive. *Catalysts* **2019**, *9*, 108. [[CrossRef](#)]
9. Acelas, N.Y.; Flórez, E. Chloride adsorption on Fe- and Al-(hydr)oxide: Estimation of gibbs free energies. *Adsorption* **2018**, *24*, 243–248. [[CrossRef](#)]
10. Xie, X.; Li, Y.; Wang, W.; Shi, L. HCl removal using cycled carbide slag from calcium looping cycles. *Appl. Energy* **2014**, *135*, 391–401. [[CrossRef](#)]

11. Lundin, L.; Gomez-Rico, M.F.; Forsberg, C.; Nordenskjöld, C.; Jansson, S. Reduction of PCDD, PCDF and PCB during co-combustion of biomass with waste products from pulp and paper industry. *Chemosphere* **2013**, *91*, 797–801. [[CrossRef](#)] [[PubMed](#)]
12. Kulkarni, P.S.; Crespo, J.G.; Afonso, C.A.M. Dioxins sources and current remediation technologies—A review. *Environ. Int.* **2008**, *34*, 139–153. [[CrossRef](#)] [[PubMed](#)]
13. Ting, C.; Chen, H.; Yen, C. A PID ratio control for removal of in flue gas from refuse municipal incinerators. *Control Eng. Pract.* **2008**, *16*, 286–293. [[CrossRef](#)]
14. Geysen, D.; Vandecasteele, C.; Jaspers, M.; Brouwers, E.; Wauters, G. Effect of improving flue gas cleaning on characteristics and immobilisation of APC residues from MSW incineration. *J. Hazard. Mater.* **2006**, *128*, 27–38. [[CrossRef](#)] [[PubMed](#)]
15. Liu, Z.S. Advanced experimental analysis of the reaction of Ca(OH)₂ with HCl and SO₂ during the spray dry scrubbing process. *Fuel* **2005**, *84*, 5–11. [[CrossRef](#)]
16. Partanen, J.; Backman, P.; Backman, R.; Hupa, M. Absorption of HCl by limestone in hot flue gases. Part III: Simultaneous absorption with SO. *Fuel* **2005**, *84*, 1685–1694. [[CrossRef](#)]
17. Partanen, J.; Backman, P.; Backman, R.; Hupa, M. Absorption of HCl by limestone in hot flue gases. Part II: Importance of calcium hydroxychloride. *Fuel* **2005**, *84*, 1674–1684. [[CrossRef](#)]
18. Partanen, J.; Backman, P.; Backman, R.; Hupa, M. Absorption of HCl by limestone in hot flue gases. Part I: The effects of temperature, gas atmosphere and absorbent quality. *Fuel* **2005**, *84*, 1664–1673. [[CrossRef](#)]
19. Ng, K.W.; Kashani-Nejad, S.; Harris, R. Kinetics of MgO chlorination with HCl gas. *Metall. Mater. Trans. B* **2005**, *36*, 405–409. [[CrossRef](#)]
20. Zhou, Q.; Tang, C.; Wang, Y.; Zheng, L. Catalytic degradation and dechlorination of PVC-containing mixed plastics via Al–Mg composite oxide catalysts. *Fuel* **2004**, *83*, 1727–1732. [[CrossRef](#)]
21. Verdone, N.; De Filippis, P. Reaction kinetics of hydrogen chloride with sodium carbonate. *Chem. Eng. Sci.* **2006**, *61*, 7487–7496. [[CrossRef](#)]
22. Nunokawa, M.; Kobayashi, M.; Shirai, H. Halide compound removal from hot coal-derived gas with reusable sodium-based sorbent. *Powder Technol.* **2008**, *180*, 216–221. [[CrossRef](#)]
23. Verdone, N.; De Filippis, P. Thermodynamic behaviour of sodium and calcium based sorbents in the emission control of waste incinerators. *Chemosphere* **2004**, *54*, 975–985. [[CrossRef](#)] [[PubMed](#)]
24. Goh, K.; Lim, T.; Dong, Z. Application of layered double hydroxides for removal of oxyanions: A review. *Water Res.* **2008**, *42*, 1343–1368. [[CrossRef](#)]
25. Yang, L.; Dadwhal, M.; Shahrivari, Z.; Ostwal, M.; Liu, P.K.T.; Sahimi, M.; Tsotsis, T.T. Adsorption of arsenic on layered double hydroxides: Effect of the particle size. *Ind. Eng. Chem. Res.* **2006**, *45*, 4742–4751. [[CrossRef](#)]
26. Cota, I.; Ramirez, E.; Medina, F.; Sueiras, J.E.; Layrac, G.; Tichit, D. Highly basic catalysts obtained by intercalation of La-containing anionic complexes in layered double hydroxides. *Appl. Catal. A Gen.* **2010**, *382*, 272–276. [[CrossRef](#)]
27. Caporale, A.G.; Pigna, M.; Azam, S.M.G.G.; Sommella, A.; Rao, M.A.; Violante, A. Effect of competing ligands on the sorption/desorption of arsenite on/from Mg–Fe layered double hydroxides (Mg–Fe-LDH). *Chem. Eng. J.* **2013**, *225*, 704–709. [[CrossRef](#)]
28. Yong, Z.; Mata, V.; Rodrigues, A.E. Adsorption of carbon dioxide onto hydrotalcite-like compounds (HTLcs) at high temperatures. *Ind. Eng. Chem. Res.* **2001**, *40*, 204–209. [[CrossRef](#)]
29. Silva, L.; Neves, V.; Ramos, V.; Silva, R.; Campos, J.; Silva, A.; Malta, L.; Senra, J. Layered double hydroxides as bifunctional catalysts for the aryl borylation under ligand-free conditions. *Catalysts* **2019**, *9*, 302. [[CrossRef](#)]
30. Abdellattif, M.; Mokhtar, M. MgAl-Layered double hydroxide solid base catalysts for henry reaction: A green protocol. *Catalysts* **2018**, *8*, 133. [[CrossRef](#)]
31. Chebout, R.; Tichit, D.; Layrac, G.; Barama, A.; Coq, B.; Cota, I.; Rangel, E.R.; Medina, F. New basic catalysts obtained from layered double hydroxides nanocomposites. *Solid State Sci.* **2010**, *12*, 1013–1017. [[CrossRef](#)]
32. Cao, J.; Chen, T.; Jin, B.; Huang, Y.; Hu, C. Structural effects of HCl adsorption on Mg–Fe hydrotalcite-like oxides at 350–650 °C in flue gas. *Ind. Eng. Chem. Res.* **2018**, *57*, 14939–14947. [[CrossRef](#)]
33. Cao, J.; Zhong, W.; Jin, B.; Wang, Z.; Wang, K. Treatment of hydrochloric acid in flue gas from municipal solid waste incineration with Ca–Mg–Al mixed oxides at medium—High temperatures. *Energy Fuel* **2014**, *28*, 4112–4117. [[CrossRef](#)]

34. Wang, J.; Liu, Q.; Zhang, G.; Li, Z.; Yang, P.; Jing, X.; Zhang, M.; Liu, T.; Jiang, Z. Synthesis, sustained release properties of magnetically functionalized organic–inorganic materials: Amoxicillin anions intercalated magnetic layered double hydroxides via calcined precursors at room temperature. *Solid State Sci.* **2009**, *11*, 1597–1601. [[CrossRef](#)]
35. He, H.; Kang, H.; Ma, S.; Bai, Y.; Yang, X. High adsorption selectivity of ZnAl layered double hydroxides and the calcined materials toward phosphate. *J. Colloid Interface Sci.* **2010**, *343*, 225–231. [[CrossRef](#)] [[PubMed](#)]



© 2019 by the authors. Licensee MDPI, Basel, Switzerland. This article is an open access article distributed under the terms and conditions of the Creative Commons Attribution (CC BY) license (<http://creativecommons.org/licenses/by/4.0/>).